

Paper I

I

SAW filter based on parallel-connected CRFs with offset frequencies

J. Meltaus, V. P. Plessky, S. Härmä,
and M. M. Salomaa

Copyright© IEEE. Reprinted with permission.

This material is posted here with permission of the IEEE. Such permission of the IEEE does not in any way imply IEEE endorsement of any of Helsinki University of Technology's products or services. Internal or personal use of this material is permitted. However, permission to reprint/republish this material for advertising or promotional purposes or for creating new collective works for resale or redistribution must be obtained from the IEEE by writing to pubs-permissions@ieee.org.

By choosing to view this document, you agree to all provisions of the copyright laws protecting it.

SAW Filter Based on Parallel-Connected CRFs with Offset Frequencies

J. Meltaus, V. P. Plessky, S. Härmä, and M. M. Salomaa

Abstract— The concept of coupled resonators is applied to synthesize surface-acoustic-wave filters. Employing two parallel-connected filter tracks, with a frequency shift imposed between them, a wide passband with low insertion loss together with well-controlled rejections is achieved. The operation of the two-track device is based on the mutual interaction of the individual transfer functions for the pair of tracks. Each track serves to contribute a part of the passband, enabling a wide band. Outside of the passband, the signals passing through the two channels may cancel each other, thus facilitating efficient control over the rejections. However, obtaining rejection stopbands at just the predetermined frequencies requires precise values for the materials parameters and a reliable fabrication process.

Prototype devices fabricated with this approach are demonstrated both on quartz and - for the first time - on 42°-LiTaO_3 . Results for two-track devices having either two or three transducers per track and operating either single-ended or with a balanced output are presented. The devices are designed employing the coupling-of-modes model and transmission-matrix approach, and the separate tracks are optimized simultaneously and independently. The center frequencies are 868 MHz and 1960 MHz. On quartz, a minimum insertion loss of 4 dB and a passband width of 0.23% are achieved at 868 MHz. On 42°-LiTaO_3 , the corresponding figures of merit are 1.3 dB for minimum insertion loss and 4.1% bandwidth at 1960 MHz. The filters on 42°-LiTaO_3 also have remarkably flat passbands.

Index Terms— Bandpass filters, Microwave filters, Surface acoustic wave filters, Surface acoustic waves.

I. INTRODUCTION

COUPLED resonator filters (CRFs) [1] have recently regained popularity compared to their ladder-type counterparts. On leaky-wave 42°-LiTaO_3 substrates with metallization thicknesses h/λ ranging from 8% to 10%, they demonstrate passband widths and minimum insertion losses (ILs) comparable to those of ladder filters, while providing improved suppression levels. CRFs can also operate with a single input and a balanced output, which is not realizable with a ladder-filter approach. Finally, at 900 MHz, CRF devices with two tracks may occupy a smaller area on the substrate than their ladder analogs having a few resonators. However, in the 1–2 GHz range the relatively large aperture of the CRF designs tends to cause increasing resistive losses.

A natural approach to minimize resistive losses is to connect two or more filters in parallel, simultaneously reducing the aperture of each track. We demonstrate that improved results can be obtained if the tracks are not equivalent but rather there is a controlled offset between the center frequencies. The optimal offset and phase difference are achieved by introducing a small difference in the pitches of the periodic transducers in each track and flipping the polarity of the output transducers in one track. A similar approach was first described by Kajihara et al. [2] and it was further discussed by the same authors [3] and by Hiramoto [4]. They propose flipping the phase of the output in one track of a two-transducer single-ended filter in order to obtain a widened passband and to improve suppression on the high-frequency side of the passband. A three-pole passband achieved using two-transducer CRF structures is sufficiently wide for most applications. However, we show that employing three-transducer designs in fact provides even further advantages: (i) an increase in the passband width and (ii) a straightforward way to obtain unbalanced-balanced (balun) operation. Since each track provides approximately one half of the final passband, the passband can be easily widened in comparison with a one-track device. To facilitate the narrower passband for one track, the number of electrodes in the transducers is higher than in a one-track CRF design. This serves also to reduce resistive losses in fingers.

We also present designs having a quasi-synchronous structure with no special gaps between the transducers; instead, we use short transducer sections between the main transducers that have a pitch different from the adjacent main transducers. This approach is discussed in [5 – 7] for standard CRF designs. Eliminating the gaps reduces the scattering and propagation losses and provides improved control over the response. Scattering to bulk acoustic wave (BAW) modes [8] is reduced since the gaps are eliminated and the structure is close to synchronous [6, 7]. Also, the short finger sections scatter predominantly at a certain frequency, as opposed to the gap that scatters over a wide band. As the pitch of the short sections is different from that of the main transducers that determine the passband, the scattering region of the short transducers lies outside of the passband.

In this paper, we discuss the performance of two-track devices on quartz and on 42°-LiTaO_3 , for the center frequencies of 868 MHz and 1960 MHz. We demonstrate balun operation for our three-transducer devices that feature a

wide band with low insertion loss and a flat passband. Combining the transfer functions of the two tracks enables a high level of control over the shape of the passband, as well as the possibility to control the rejections and to form rejection stopbands. We also study the operation of the two-track structure and discuss the main issues to be observed in design. Some of these results are presented in [9].

II. DEVICE DESIGN AND SIMULATIONS

We have designed devices with the two parallel-connected tracks consisting of two-transducer and three-transducer CRFs. Both tracks are optimized simultaneously and independently. The COM optimization procedure was applied to an equivalent single-ended device. The substrate materials employed are quartz (for the two-transducer designs) and 42° -LiTaO₃ (for the three-transducer designs).

A. Theoretical Background

In the optimization of the devices, we employ the coupling-of-modes (COM) model [10] and transmission-matrix representation [11]. In the COM model, the wave field in the structure is described as two counter-propagating modes. The COM equations can be expressed as

$$\begin{cases} \frac{dR(x)}{dx} = -j\delta R(x) - j\kappa S(x) + j\alpha V \\ \frac{dS(x)}{dx} = j\kappa^* R(x) + j\delta S(x) - j\alpha^* V \\ \frac{dI(x)}{dx} = -2j\alpha^* R(x) - 2j\alpha S(x) + j\omega CV, \end{cases} \quad (1)$$

where $R(x)$ and $S(x)$ are slowly varying acoustic fields, V and I are the voltage and the current in the device, respectively, and δ , κ , and α are the coupling-of-mode parameters. Solving Eq. (1) with the boundary conditions that the waves entering the structure are known yields the transmission matrix H . For a device that has two acoustic ports and N electrical ports (Fig. 1), H is an $2N+2 \times 2N+2$ matrix such that

$$\begin{pmatrix} R(L) \\ S(L) \\ V_1(L) \\ I_1(L) \\ V_2(L) \\ \vdots \\ I_N(L) \end{pmatrix} = \begin{pmatrix} H_{11} & H_{12} & H_{13} & \cdots & H_{1,2N+2} \\ H_{21} & H_{22} & \cdots & & H_{2,2N+2} \\ \vdots & & \ddots & & \vdots \\ H_{2N+2,1} & \cdots & & & H_{2N+2,2N+2} \end{pmatrix} \begin{pmatrix} R(0) \\ S(0) \\ V_1(0) \\ I_1(0) \\ V_2(0) \\ \vdots \\ I_N(0) \end{pmatrix}. \quad (2)$$

The values for the matrix elements are obtained from the solution of the COM equations. Transmission matrices provide a straightforward method for acoustically connecting several SAW elements such as reflectors, transducers, and gaps. Thus, they are extremely useful for the design of multi-transducer CRFs.

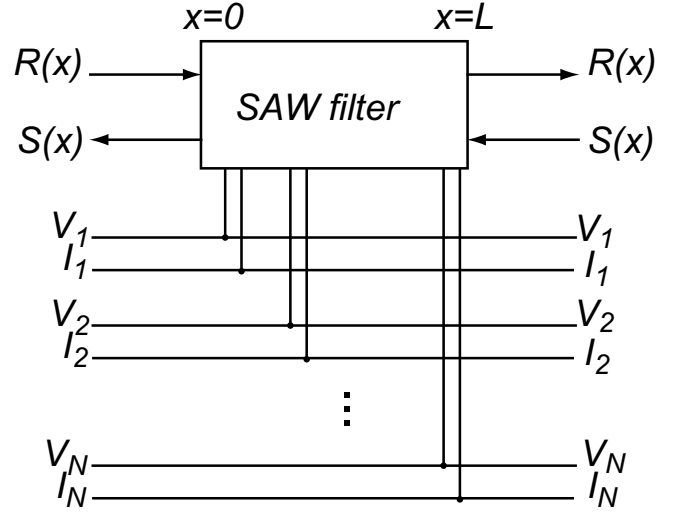


Fig. 1. A SAW device that has two acoustic ports and N electrical ports. Voltages and currents in each port are denoted by V_n and I_n . The acoustic field in the structure is described with two counter-propagating, slowly varying modes R and S .

Considering a three-transducer device, shown schematically in Fig. 2 below, we have two CRF tracks connected in parallel. In each track, the phase of output 1 is flipped with respect to that of output 2 so as to obtain a balanced output. In addition to that the phases of the outputs are flipped between the two tracks. Fig. 2 shows the “distributed gap” design, where the conventional gaps between the transducers are replaced with short IDT sections having their pitches different, preferably smaller, from that of the “main” IDTs. In this way, the gap is effectively “distributed” over the length of the short transducers. The structure is quasi-synchronous, appearing as having no special gaps at all, with the exception of the gap between the reflector and the first transducer. The center-to-center distance of the adjacent electrodes having different pitches is $(pt1+pt2)/2$. A similar technique is described in patents [5 – 7].

The design methodology of this type of parallel-connected device for narrow-band devices has been considered, for example, in [2-4, 12]. To obtain a wide bandwidth, the resonances of the two tracks are designed to overlap, with the phases of the resonances matching. This is illustrated in Fig. 3 for an actual device design with a structure similar to that shown in Fig. 2. In Fig. 3, the resonances of the two tracks are shown in mismatched ($1-\Omega$) environment, calculated using the COM model. Track 1 (plotted with solid line) has a 2-pole response, whereas track 2 (dashed line) shows a 2-pole response with auxiliary smaller resonances at each side, shifted upwards in frequency compared to track 1. So as to match the phases of the overlapping resonance peak, the phases in the outputs of the tracks are flipped with respect to one another, as shown in Fig. 1.

Employing the distributed gaps instead of metallized gaps, as illustrated in Fig. 2, yields a reduction in the insertion loss of the device, arising from decreased free-surface propagation loss (on 42° -LiTaO₃) and minimized scattering into bulk

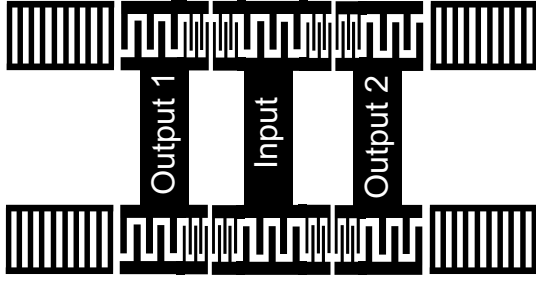


Fig. 2: Schematic of a 3-IDT design with distributed gaps. Phases in the output transducer in each track are flipped to provide balanced output; in addition, output phase of track 2 is flipped with respect to that in track 1.

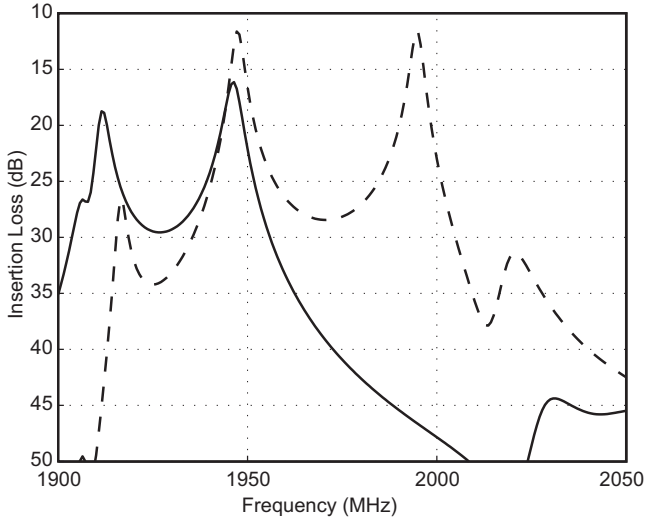


Fig. 3: COM simulation of two 3-IDT tracks in a mismatched environment (1Ω). The first track (solid line) has a 2-pole response, whereas the second track has a 2-pole response with two auxiliary smaller peaks. To match the phases of the overlapping resonance in the two tracks, the polarity of the output in the second track is flipped.

waves. For leaky waves on 42°-LiTaO_3 , the propagation loss is close to zero when the wave propagates on a grating with metal thickness of $0.07\text{-}0.1\lambda$, but increases approximately to $0.008 \text{ dB}/\lambda$ for propagation on free or metallized surface [13]. This effect is especially important at high frequencies. Moreover, any discontinuities in the periodicity in the propagation path of the wave, such as transducer edges at a gap, cause scattering of the surface wave into bulk wave, leading to increased loss. Eliminating the gaps makes the discontinuities less prominent, resulting in a “quasi-synchronous” structure.

B. Simulations

The devices were optimized using the COM model. For simplicity, balanced structures were optimized as single-ended. It should be noted here that the COM model cannot take into account the bulk scattering effect described above. The increased loss in the gaps was phenomenologically included in the model.

1) Two-Transducer Design

A two-transducer device [2–4] allows a simple interconnection topology. Fig. 4 is a schematic of a single-ended two-transducer device with two tracks connected in parallel,

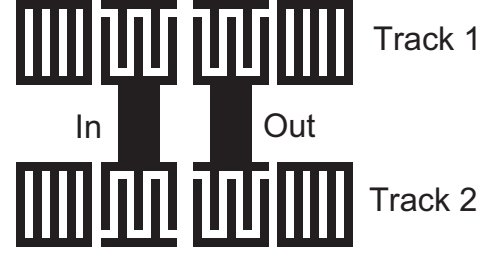


Fig. 4: Schematic of a two-transducer device, similar to that presented in [2]. Tracks are connected in parallel and the polarity of the output transducer in track 2 is flipped with respect to that in track 1.

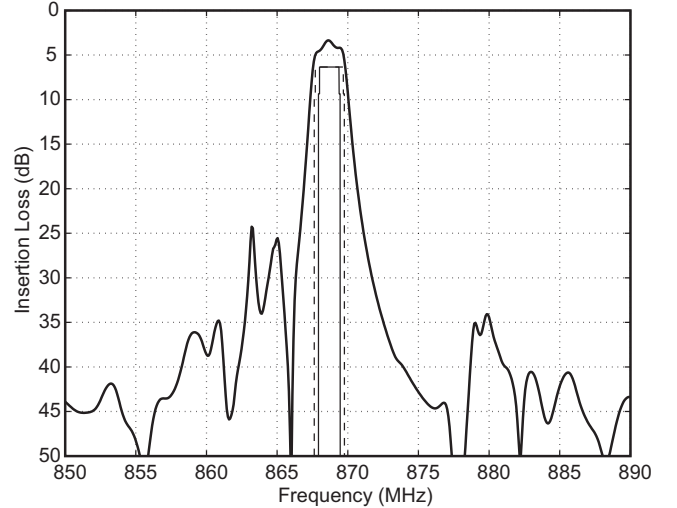


Fig. 5: COM simulation of the two-transducer design in Fig. 4 on quartz. The center frequency is 868 MHz and the bandwidth is 2 MHz (0.2%).

similar to that presented in [2]. Note that the polarity of the output transducer in track 2 is flipped with respect to that of track 1. This will not, however, yield balanced output, since the response of track 2 is frequency-shifted with respect to that in track 1, so that at certain frequencies only one track is effectively in resonance (see Fig. 3). Achieving balanced output is possible but finding a symmetrical topology may not be straightforward.

Fig. 5 illustrates a simulation result for a single-ended two-transducer device on quartz. The design is an ISM-band filter with the center frequency at 868 MHz and a relative 3-dB bandwidth of 2 MHz (0.2%). The simulated minimum insertion loss is 3.5 dB.

2) Three-Transducer Design

In addition to a wide passband and a high suppression level, a three-transducer design further provides a straightforward way of achieving unbalanced-balanced operation. We have studied here the structure illustrated in Fig. 2, having an unbalanced input and balanced output. In what follows, we consider two types of track design: one has metallized gaps between the transducers, whereas in the other, the gaps are replaced with short transducers, as shown in Fig. 2. The devices are designed for $50\text{-}\Omega$ input and $150\text{-}\Omega$ output.

Metallized Gaps: In the simplest CRF scheme, the transducers are separated by gaps, as illustrated in Fig. 4.

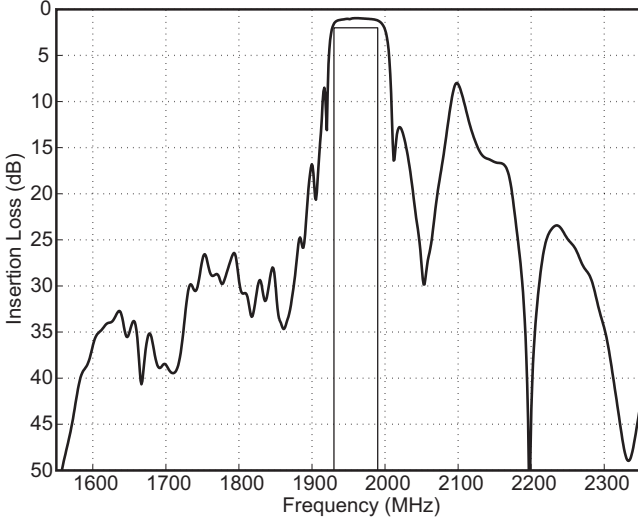


Fig. 6: COM simulation of the three-transducer design with metallized gaps on 42°-LiTaO_3 .



Fig. 7: Simulation of a three-transducer design with distributed gaps on 42°-LiTaO_3 . The passband is slightly wider than in the metallized-gap design due to minimized gap loss.

Typically, the gaps are metallized in order to minimize the propagation losses arising from the waves traversing an open surface. The propagation losses occurring in the gap were included in the optimization. Fig. 6 depicts a COM-model simulation of a three-transducer device with metallized gaps. The apertures of the tracks are $53\ \mu\text{m}$ and $68\ \mu\text{m}$ and the finger width is approximately $0.6\ \mu\text{m}$. The substrate material is 42°-LiTaO_3 . The simulated center frequency is $1960\ \text{MHz}$ and the absolute 3-dB bandwidth is $65\ \text{MHz}$ (3.3%).

Distributed Gaps: As described above in section 2.1, losses can be reduced by replacing the metallized gaps with short transducer sections (“distributed gaps”) as shown in Fig. 2. Fig. 7 shows a simulated response for a three-transducer device with distributed gaps on 42°-LiTaO_3 . The apertures of the tracks are $55\ \mu\text{m}$ and $70\ \mu\text{m}$ and the finger width is approximately $0.6\ \mu\text{m}$. The number of fingers in the short IDT sections is 4. The simulated response has a center frequency of $1960\ \text{MHz}$ and a wide bandwidth of $85\ \text{MHz}$ (4.3%). The simulated passband is quite flat.

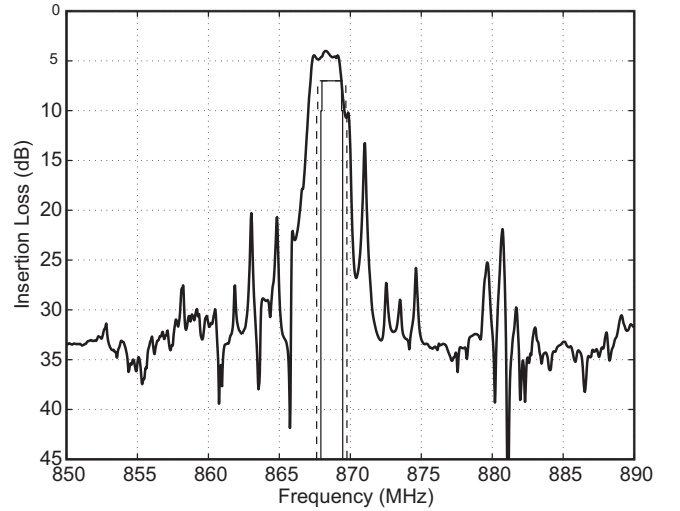


Fig. 8: Experimental data for a four-track two-transducer design on quartz. Measurement agrees well with the simulation. Parasitic transverse modes appear on the right side of the passband.

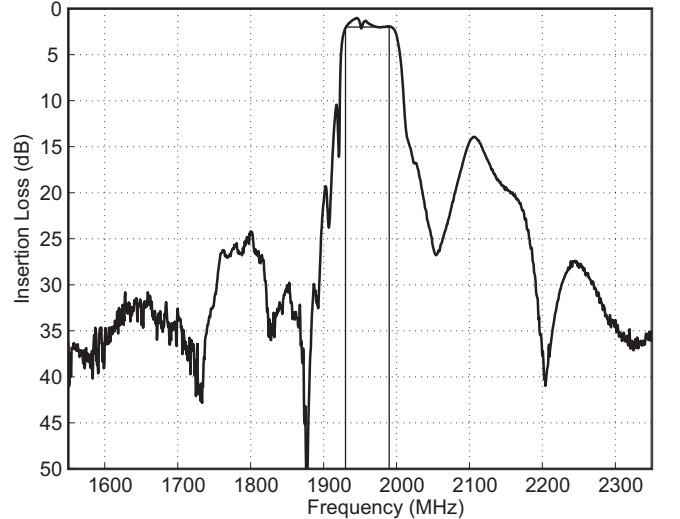


Fig. 9: Measured response of a three-transducer design with metallized gaps on 42°-LiTaO_3 .

III. EXPERIMENTAL RESULTS

We have fabricated and measured several different CRF devices on quartz and 42°-LiTaO_3 . We have designed structures with two or three transducers in each track and having metallized or distributed gaps. We demonstrate both single-ended and balun devices.

A. Two-Transducer Device

Fig. 8 shows the measured response for the device simulated in Fig. 5. To further reduce the aperture, two identical pairs of tracks as depicted in Fig. 4 were connected in parallel, in effect leading to a four-track design. The substrate is quartz and the aluminum electrode thickness is $80\ \text{nm}$ ($h/\lambda = 2.2\%$).

The measured curve agrees well with the COM simulation. The center frequency is slightly shifted downwards but the relative 3-dB bandwidth is still $2\ \text{MHz}$ (0.2%). The measured minimum insertion loss is $4\ \text{dB}$. The slightly decreased

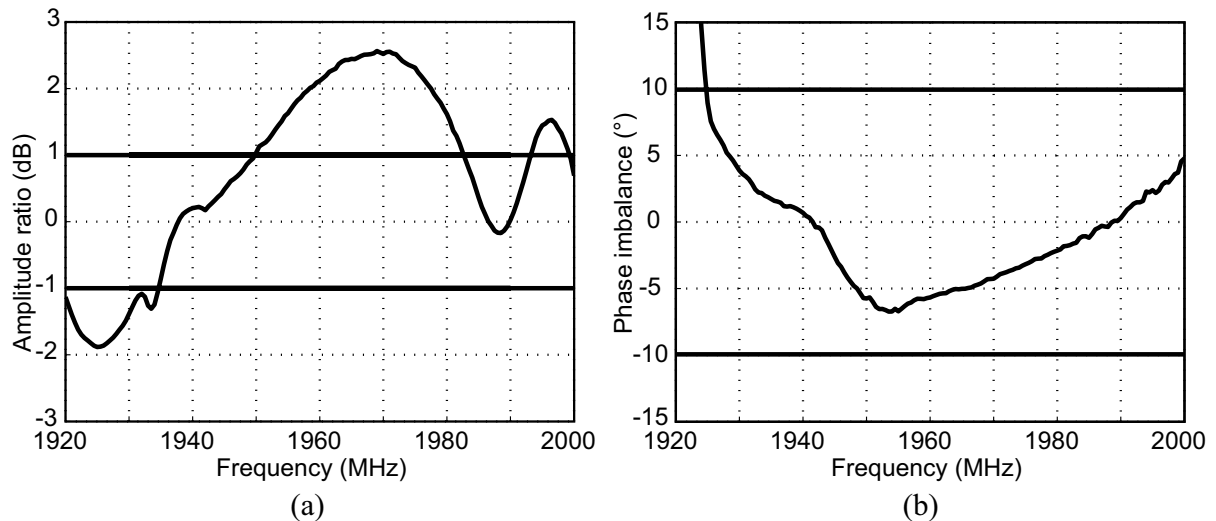


Fig. 10: Balance characteristics for the three-transducer design with metallized gaps. Amplitude ratio (a) and phase balance (b) are plotted here. The measured response for the device is plotted in Fig. 9.

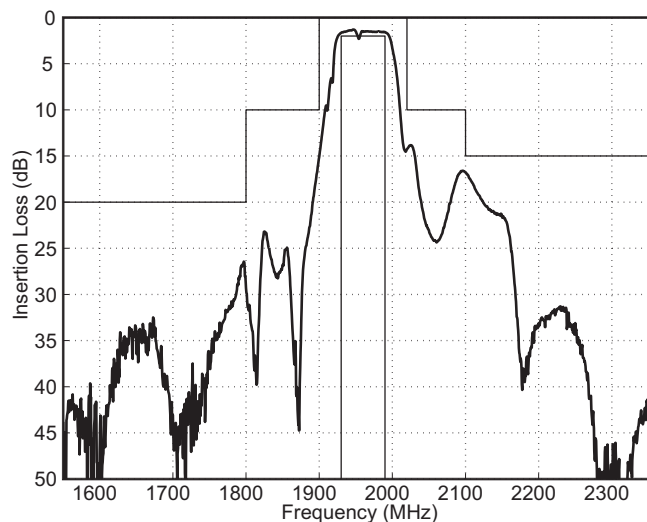


Fig. 11: Measured response of a three-transducer device with distributed gaps on 42°-LiTaO₃.

suppression levels in the measurement are interpreted to result from feedthrough arising from the device layout. There remain parasitic transverse modes appearing on the right side of the passband, despite the narrow aperture used. The measured curve is matched to 50/50 Ω with 18 nH in series and 2.3 pF in parallel at both input and output.

B. Three-Transducer Device

In the measurements for the three-transducer devices, the substrate is 42°-LiTaO₃ with a relative metallization thickness $h/\lambda = 8\%$. The devices were designed for 50/150 Ω , but final matching was slightly better for 50/250 Ω , with 10 nH parallel to output. These impedances are used in the figures in this section.

1) Metallized Gaps

Fig. 9 represents the measured response of a CRF device with metallized gaps. Comparison with the simulated response in Fig. 6 indicates that the agreement between the device modeling and the actual measurement is very close. The

appearance of the notch in the middle of the passband is due to the fact that the COM parameters used in design slightly differ from the actual COM parameters corresponding to the electrode structure realized on the lithium tantalate substrate. This discrepancy leads to a modification of the resonance conditions of the tracks, resulting in an imperfect coverage of the passband; see the next section for a more detailed explanation of the effect. The response depicted in Fig. 9 features a center frequency of 1960 MHz, an absolute 3-dB bandwidth of 73 MHz (3.7%) and a minimum insertion loss of 1.0 dB.

As seen in Fig. 10, the balance characteristics of the device are not perfect. Imperfect balance arises mainly from parasitic capacitances firstly between the adjacent signal fingers in the active structure itself and secondly between the input and the output bond pads. At high frequencies (~ 2 GHz and higher), the effect of the parasitic capacitances is emphasized. To improve the balance, the parasitics arising from the structure must be incorporated in the optimization procedure and minimized, and the layout of the device must be such that parasitics arising from the bond pad configuration are as small as possible.

2) Distributed Gap

Fig. 11 represents a measurement result of the frequency response for a three-transducer device with distributed gaps. Compared with Fig. 7, the correspondence with the simulation is excellent. The passband is exceedingly flat, except for the notch in the middle of the passband; its origins are described in the following section. The absolute 3-dB bandwidth is 80 MHz (4.1%) and the minimum insertion loss is 1.3 dB.

Compared with the response of the metallized-gap device depicted in Fig. 9, the distributed-gap device has a wider and flatter passband and lower average insertion loss. These improvements arise from the elimination of the discontinuities in the structure (gaps) that leads to a reduction in the propagation and scattering losses.

The balance characteristics of the distributed-gap device are

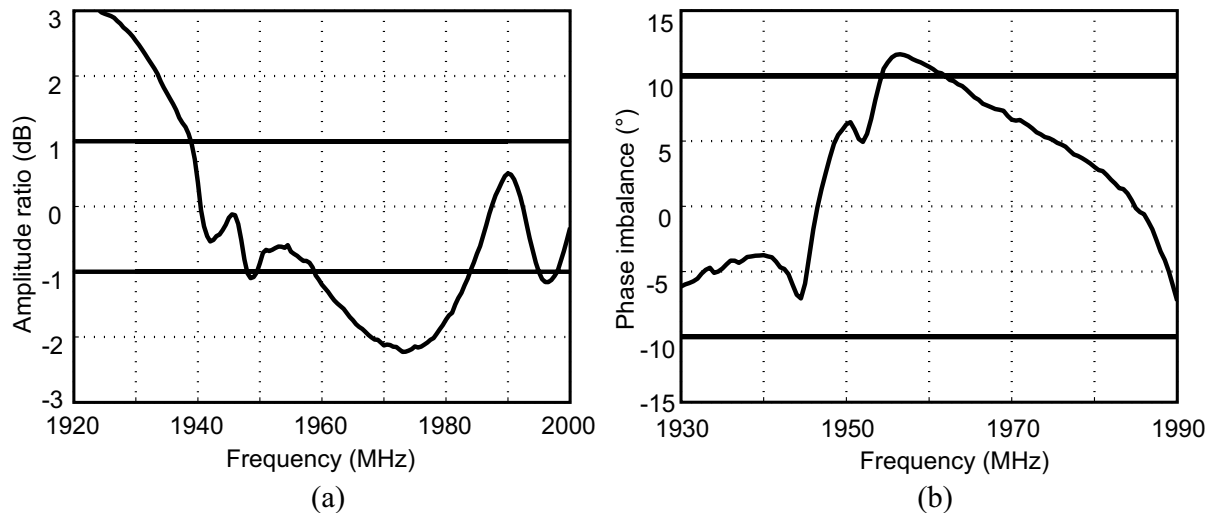


Fig. 12: Balance characteristics of the three-transducer device with distributed gaps. Amplitude ratio (a) and phase balance (b) are plotted here. The measured response of the device is presented in Fig. 11.

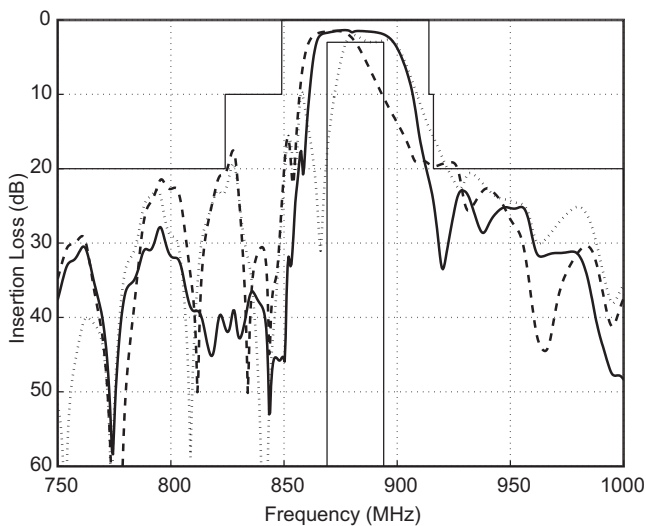


Fig. 13: Simulation of the operation principle of the two-track devices. Track 1 (dashed curve) and track 2 (dotted curve) act together to create the final filter response (solid curve).

comparable to those of the metallized-gap device. The same arguments apply to the both designs, and the same methods can be employed to improve the balance.

IV. TWO-TRACK OPERATION AND DESIGN CONSIDERATIONS

In the parallel-connected two-track structure, each track is responsible for a part of the final passband. To illustrate the operation of the structure and the effect of various parameters on the final response, we consider a metallized-gap device such as that described in Fig. 4 on 42°-LiTaO_3 , working at the center frequency of 881 MHz. The operation of the tracks is illustrated by a simulation in Fig. 13. The first track (dashed curve) and the second track (dotted curve) produce independent responses, which then interact to create the final filter response (solid curve). As portrayed in Fig. 13, each track creates a narrow passband at a different center frequency: track 1 operates at lower frequency and track 2 at higher frequency. Changing one or both of the separate passbands

slightly affects the total response, typically creating a notch at the frequency where the dominating track response is swapped. The creation of the notch is illustrated in Fig. 14, where the width of the gap between the transducers is decreased by 3% in both tracks. This decrease leads to a shift in the resonance condition of the track, resulting in the notch at the point where the two passbands no longer completely overlap. In Figs. 15 - 17, the simulated (Fig. 15) and measured (Figs. 16 and 17) effects of modifying the gap by $\pm 3\%$ are illustrated. As Figs. 16 and 17 show, the gap controls the appearance of the notch, but does not affect the suppressions. This is because the passband is essentially determined by the resonances that arise in the gap region, but the shape of the stopband is mainly governed by other parameters.

Achieving a perfectly smooth response in the passband requires an accurate knowledge of the COM parameters – a small error in the parameters used in the optimization may result in the appearance of the notch, as the resonance conditions of the tracks are changed.

In Fig. 13, the final suppression (solid curve) on the left side of the passband is at -35 dB level. However, as seen from the curves describing the two tracks separately, each track by itself has a peak of -20 dB at this frequency range. The destructive interaction of the two transfer functions leads to the improved suppression. However, if one of the tracks is slightly changed, the cancellation of the peaks ceases to be perfect and the suppression is decreased. This is illustrated in Figs. 18 - 20. In Fig. 18, a COM simulation of the effect is shown. In one of the tracks, all the pitches of the transducers are changed by ± 2 nm. The modification of the pitches leads to the corresponding track's response shifting in frequency, which destroys the cancellation of the peaks. The resulting filter-response curves (dashed for -2 nm and dash-dotted for +2 nm) have a deteriorated suppression level. In Figs. 19 and 20, this effect is verified experimentally. Changing the pitches also affects the passband: as one track is slightly shifted, a notch may appear at the track response overlap region in the passband.

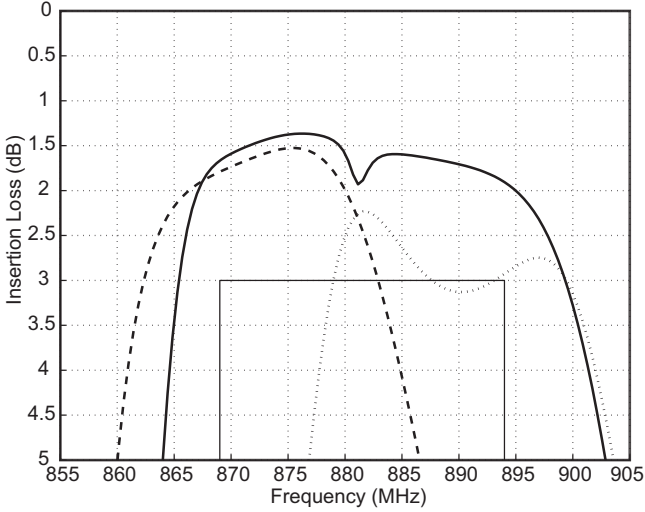


Fig. 14: Simulated illustration of the appearance of the notch in the two-track response. In track 1 (dashed curve) and track 2 (dotted curve), the gap between the transducers is decreased by 3%. A relatively small modification of the gap results in a notch in the passband of the total response (solid curve).

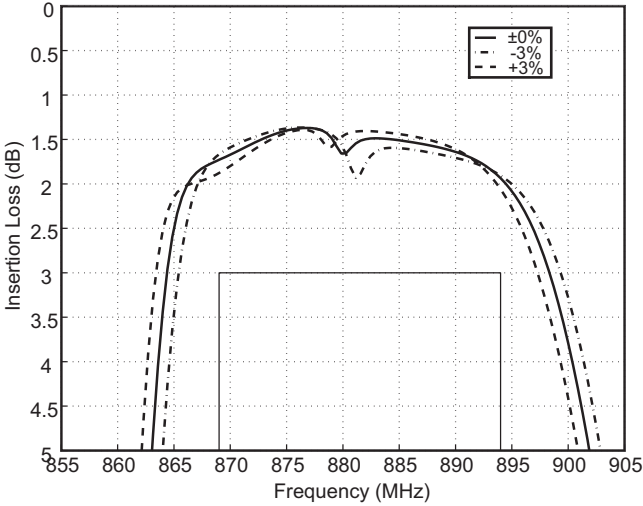


Fig. 15: Behavior of the depth and the position of the notch as a function of the length of the gaps. The effect is simulated by modifying the gaps in both tracks by $\pm 3\%$.

In summary, we note that in the metallized-gap device, the gaps determine the overlap of the two tracks in the passband. Transducer pitches mainly control the suppressions through the cancellation of the two transfer functions, although changing the pitches naturally has some effect on the passband as well. In a distributed-gap device, the same conclusions apply, except that the pitches of the short intermediate transducers now have the role of the gaps.

Accurately achieving the desired filter response requires a detailed knowledge of the COM parameters as well as a reliable fabrication process – a very small error in the parameters leads to a relatively large change in the response, as seen in Fig. 20.

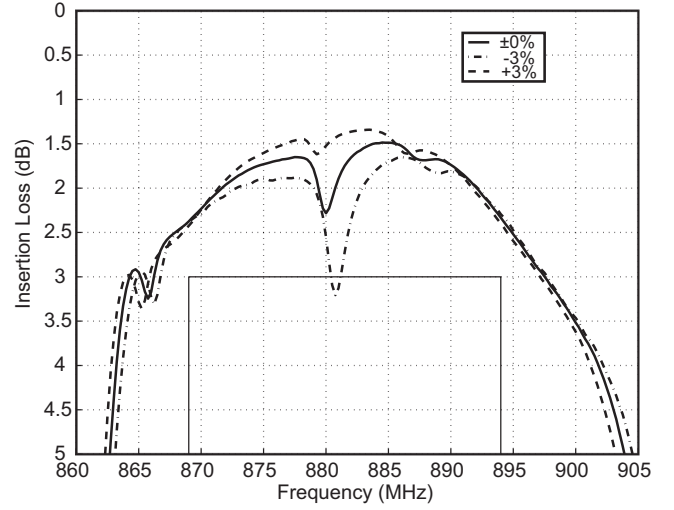


Fig. 16: Measured result of modifying the metallized gaps in both tracks by $\pm 3\%$. Comparing Figs. 15 and 16 shows that in reality the effect is more pronounced than in simulation.

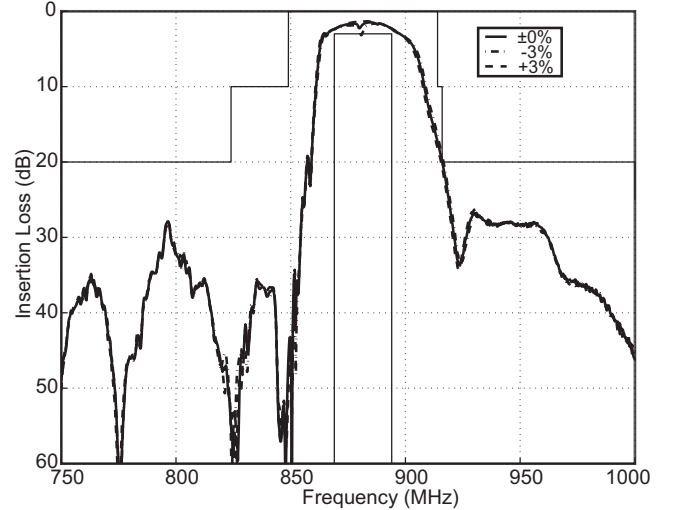


Fig. 17: Measured effect of modifying the metallized gaps in both tracks by $\pm 3\%$, wide-band. Apart from the appearance of the notch in the passband, the response is not significantly affected.

V. DISCUSSION

We have demonstrated that connecting two tracks in parallel with offset frequencies and flipped phases at the output yields an improved frequency response. In particular, employing a three-transducer design provides simple means of obtaining unbalanced-balanced operation with excellent performance with respect to insertion loss, passband width and the flatness of the passband. The improvement in the insertion loss results from the decreased resistive losses due to the narrower aperture. The fact that each track features a larger number of electrodes than a standard CRF is also an advantage – it leads to a reduction of the resistive losses, simultaneously rendering the losses in the gaps relatively less important. The propagation and scattering losses arising from the gaps can be significantly reduced if the gaps are replaced with short transducers that have a pitch different from the main

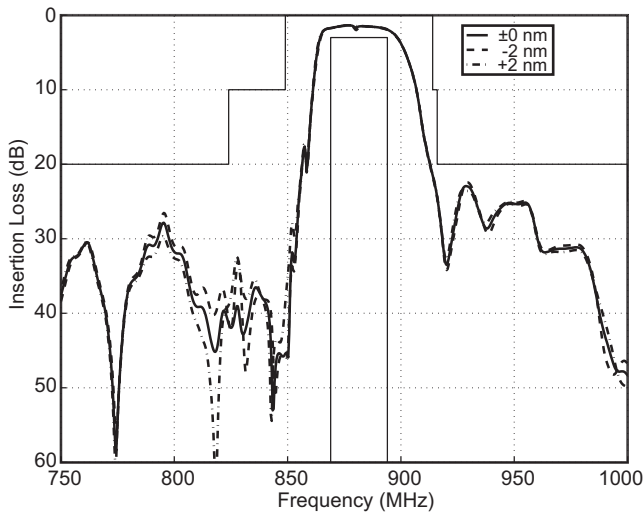


Fig. 18: Simulation of the effect of modifying the pitches in the upper-frequency track by ± 2 nm. Solid line: total filter response for the original design. Dashed line: total filter response for the design with reduced pitches in one track. Dash-dotted line: total filter response for the design with increased pitches in one track. Changing the pitches in the transducers mainly affects the suppressions on the left side of the passband.

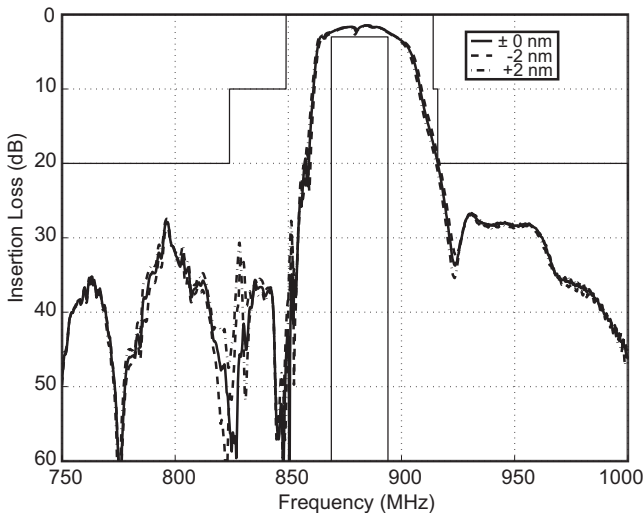


Fig. 19: Measured effect of the modification of the pitches in the upper-frequency track by ± 2 nm. Solid line: original curve, dashed line: reduced pitches, dash-dot line: increased pitches. The suppression in the stopband on the left side of the passband is reduced as the result of the change in the pitches.

transducers. Results of this distributed-gap device demonstrate a widened, very flat passband with a reduced insertion loss. Agreement between simulations and measurements is good.

The improvement in the rejection levels compared to a one-track CRF device originates from a cancellation of the transfer functions of the two tracks. Therefore, achieving strong rejections at exactly the predetermined frequency (especially in the form of frequency stopbands) may prove to be challenging, and requires a reliable fabrication technology.

The combination of the two passbands provided by the two tracks into a single flat passband requires an accurate knowledge of the materials parameters. Even a small error in the offset between the frequencies of the tracks may result in a notch in the middle of the passband. These drawbacks are the

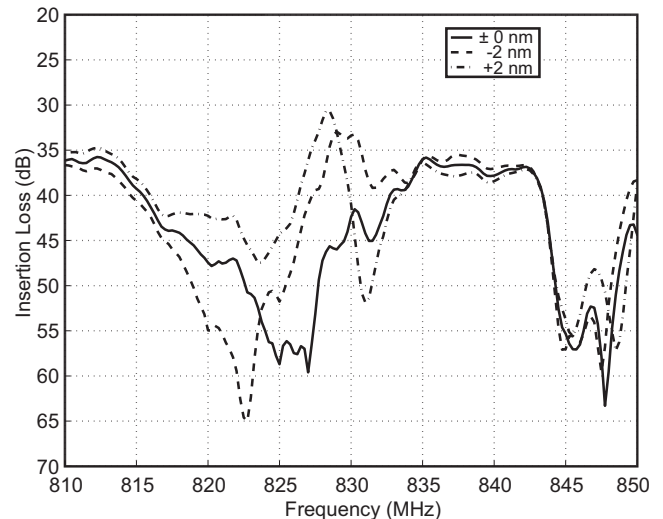


Fig. 20: Close-up on the effect of pitch modification, measured response. The suppression is reduced at most by 15 dB.

tradeoff for achieving a low loss in the passband.

The approach presented in this paper can be applied to a wide range of frequencies and to several applications in telecommunications, including GSM and ISM band applications. Our approach is especially appropriate for situations where the principal aim is a low loss level in the passband.

ACKNOWLEDGMENT

The authors thank Clinton Hartmann for help and pertinent interest in this work, A. Gortchakov for measurements of the 868 MHz devices, and Paul Brown and William Bonner for the measurements of the 881 MHz and 1.9 GHz devices.

REFERENCES

- [1] T. Morita, Y. Watanabe, M. Tanaka, and Y. Nakazawa, "Wideband low loss double mode SAW filters", in Proc.1992 IEEE Ultrasonics Symposium, pp. 95-104.
- [2] Y. Yamamoto and R. Kajihara, "SAW composite longitudinal mode resonator (CLMR) filters and their application to new synthesized resonator filters", in Proc.1993 IEEE Ultrasonics Symposium, pp. 47-51.
- [3] Y. Yamamoto, R. Kajihara, and S. Yoshimoto, "SAW synthesized resonator filters with two composite longitudinal mode 2-port resonators", in Proc.1998 IEEE Ultrasonics Symposium, pp. 91-95.
- [4] M. Hiramoto, "Surface acoustic wave resonator filter with longitudinally coupled resonators having specific resonance frequency placements", US Patent 5,909,158, June 1, 1999.
- [5] T. Bauer, G. Kovacs, U. Rösler, and W. Ruile, "Surface acoustic wave arrangement with a junction region between surface acoustic wave structures having a decreasing then increasing finger period", US Patent 6,420,946, July 16, 2002.
- [6] Y. Takamine, "Longitudinally coupled resonator type surface acoustic wave filter with an IDT having a narrow pitch portion", US Patent 6,583,691, June 24, 2003.
- [7] Y. Takamine, "Longitudinally coupled resonator type surface acoustic wave filter having narrow electrode finger pitch sections", US Patent 6,621,380, Sep. 16, 2003.
- [8] D. P. Morgan, *Surface-Wave Devices for Signal Processing*, Elsevier, Amsterdam, 1991.
- [9] J. Meltaus, V. P. Plessky, A. Gortchakov, S. Härmä, and M. M. Salomaa, "SAW filter based on parallel-connected CRFs with offset frequencies", in Proc.2003 IEEE Ultrasonics Symposium, pp. 2073-2076.

- [10] V. P. Plessky and J. Koskela, "Coupling-of-modes analysis of SAW devices", *Int. J. High Speed El. and Syst.*, vol. 10, no. 4, pp. 867-947, Dec. 2000.
- [11] K.-Y. Hashimoto, *Surface Acoustic Wave Devices in Telecommunications: Modelling and Simulation*, Springer-Verlag, Berlin, 2000.
- [12] A. N. Rusakov, J. D. Dai, and R. J. Kansy, "Design of wide band SAW coupled resonator filters on quartz", in *Proc. 2003 IEEE Ultrasonics Symposium*, pp. 513-517.
- [13] O. Kawachi, S. Mineyoshi, G. Endoh, M. Ueda, O. Ikata, K. Hashimoto, and M. Yamaguchi, "Optimal cut for leaky SAW on LiTaO₃ for high performance resonators and filters", *IEEE Trans. Ultrason. Ferroelect. Freq. Contr.*, vol. 48, pp. 1442-1448, Sep. 2001.